

PAPER

## Nonlinear guided waves for fatigue crack evaluation in steel joints with digital image correlation validation

To cite this article: Yu Fung Lee *et al* 2020 *Smart Mater. Struct.* **29** 035031

View the [article online](#) for updates and enhancements.

### You may also like

- [Modelling and analysis of nonlinear guided waves interaction at a breathing crack using time-domain spectral finite element method](#)  
Shuai He and Ching Tai Ng
- [Investigation of textured sensing skin for monitoring fatigue cracks on fillet welds](#)  
Han Liu, Simon Laflamme, Jian Li et al.
- [A review of non-axisymmetric guided waves and their corresponding transducers for defect detection in circular tube structures](#)  
Zhou Fang



**PRIME**  
PACIFIC RIM MEETING  
ON ELECTROCHEMICAL  
AND SOLID STATE SCIENCE

HONOLULU, HI  
Oct 6–11, 2024

Abstract submission deadline:  
**April 12, 2024**


**Learn more and submit!**

**Joint Meeting of**

The Electrochemical Society  
•  
The Electrochemical Society of Japan  
•  
Korea Electrochemical Society

The banner features a collage of images showing people at a conference, including a woman in the foreground and others in the background looking at posters.

# Nonlinear guided waves for fatigue crack evaluation in steel joints with digital image correlation validation

Yu Fung Lee, Ye Lu<sup>1</sup>  and Ruiqi Guan

Department of Civil Engineering, Monash University, Clayton VIC 3800, Australia

E-mail: [ye.lu@monash.edu](mailto:ye.lu@monash.edu)

Received 21 July 2019, revised 19 November 2019

Accepted for publication 24 January 2020

Published 12 February 2020



## Abstract

This paper presents a study of nonlinear guided-wave-based fatigue crack identification in a steel joint subjected to tensile fatigue loadings. The steel joint is considered as a section of a railway bogie, a vital component of the train structure. Finite element method and experiment were used to evaluate fatigue crack based on the second harmonic method. The symmetric mode (S1) of Lamb waves was selected as the input signal and excited in experiment by piezoelectric transducers installed on the upper surface of the joint. The sensing paths were aligned perpendicularly to and at various distances from the potential crack trajectory. When the waves interacted with the crack, higher order harmonics were produced owing to the phenomenon of contact acoustic nonlinearity. A nonlinear index based on the second harmonic characteristics was exploited to define the nonlinearity. To validate the outcomes based on nonlinear guided waves, a digital image correlation technique was implemented and the results were in good agreement. The findings indicated that the nonlinear guided-wave-based technique is capable of identifying crack initiation and growth in such joint type structures.

Keywords: nonlinear guided waves, fatigue crack, digital image correlation

(Some figures may appear in colour only in the online journal)

## 1. Introduction

The volume of both freight and passengers delivered by rail transport in Australia has risen considerably over the last decade [1] due to the cost-effectiveness and large coverage of rail to regional areas compared with other transport modes. Owing to population and economic growth, faster and higher capacity rail, along with railway network extension, is in demand to facilitate the increasing number of commuters, all of which impose a higher possibility of fatigue failure in crucial railway components. The consequences of poor maintenance can be severe: service breakdown, disruptions to hundreds of thousands of commuters, even train crashes that can cause passenger fatalities and injuries. The railway bogie, located underneath and near the ends of railway carriages, is a vital component of the train, holding the axles, suspension

and brakes. Despite the fact that the examination of train components is indeed executed on a regular basis, i.e. schedule based, disturbance to usual train services is inevitable and there is no scientific evidence to support a cost-effective inspection interval so that disastrous failures can be prevented. Moreover, existing nondestructive approaches for assessing bogie condition, such as exterior visual inspection, which requires lifting the train or disassembling the car body, magnetic particle inspection to visually ascertain damage [2], and evaluation of the contact forces between wheel and rail through strain gauges [3] are inefficient because they are limited to identify macro-damage and are time-consuming.

In response to the inefficiencies of existing technologies, a condition-based philosophy has been introduced to provide continuous and automated surveillance of structures with the assistance of instrumented transducers/sensors, known as structural health monitoring (SHM). In particular, SHM techniques, based on ultrasonic guided waves which can

<sup>1</sup> Author to whom any correspondence should be addressed.

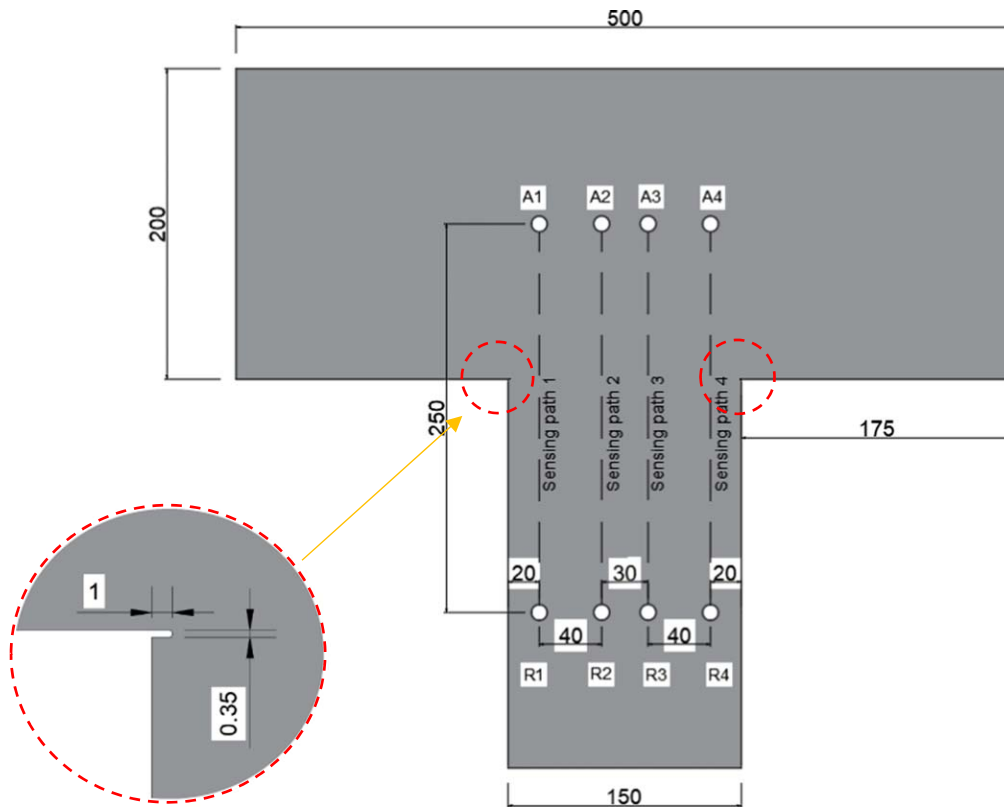


**Figure 1.** Geometry of the T-shaped plate and the locations of actuators and sensors (in mm).

propagate over a reasonably long distance in structures, are successful in identifying various types of damage, including delamination [4], crack [5] and debonding [6] in many engineering structures. In this respect, guided wave techniques have been well established for damage detection by monitoring the variations of linear characteristics such as the delay in time of flight, wave reflections or scattering, and energy dissipation. Guided wave techniques have been used for damage detection in pipelines [7], rail track [8] and aircraft wings [9]. However, current methods using linear wave features are generally limited by the wavelength of the selected wave mode. They can only detect macro-damage of dimensions comparable to the wavelength but cannot detect micro-structural defects or defect initiation.

Given the limitations of linear guided waves and the need to recognise damage in its earliest stage, the nonlinear guided-wave-based method offers an alternative for detecting and monitoring the initiation and growth of micro-damage. Much research has been undertaken to detect impairments based on nonlinear wave components in various materials and structures experimentally such as aluminium plate [10] and pipe [11], steel plate [12] and shafts [13], composites [14], meta-material [15], FRP-reinforced steel [16] and bolt joints [17]. However, current research using nonlinear guided waves is mainly focused on qualitative study of damage, whereas quantitative damage assessment is less reported [18–20] yet but conversely important for SHM with the aim of monitoring damage severity.

On the other hand, it is well known that the digital image correlation (DIC) technique [21] is able to measure full-field

**Table 1.** Material parameters.

Elastic modulus (GPa)	Density ( $\text{kg m}^{-3}$ )	Poisson's ratio	Thickness (mm)
210	7850	0.3	10

deformation based on the difference between the reference image and images captured subsequently. This technique has been extensively employed to quantify the surface displacement field in different materials (e.g. nickel-based superalloy [22], GFRP laminates [23] and masonry walls [24]), and to determine the mechanical properties of material (e.g. coefficient of thermal expansion [25], stress intensity factors [26] and Young's modulus [27]). DIC has also been incorporated with conventional ultrasonic inspection to detect bonding condition in adhesive joints [28] and to monitor damage processes in rocks under axial load [29], and has been combined with acoustic emission to monitor crack in concrete structures [30]. In light of its sensitivity and robustness for small deformation measurement, DIC technique will be implemented in this study as a supplementary tool to facilitate the interpretation of the results from nonlinear guided waves for the quantification of fatigue crack.

In this paper, nonlinear Lamb waves were employed for quantitative fatigue crack evaluation in a steel joint, which was considered as a section of bogie frame. Numerical simulation and experimental tests were conducted to verify the method's feasibility, and the DIC technique was deployed to support the findings. This paper is organised as follows:

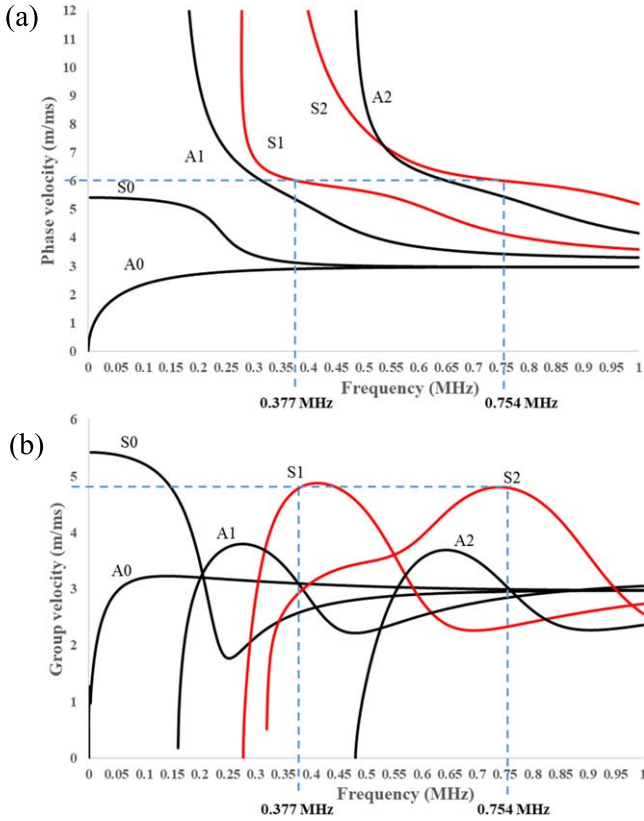


**Figure 2.** Dispersion curves of (a) phase velocities and (b) group velocities.

section 2 presents the theoretical principle of nonlinear Lamb waves. Numerical modelling is elaborated in section 3, followed by an experimental study of fatigue crack detection in a joint using both nonlinear Lamb waves and DIC in section 4. Finally, discussion and conclusions are presented.

## 2. Wave nonlinearity and contact acoustic nonlinearity (CAN)

When guided waves travel in a medium with a fatigue crack, higher harmonics of the excitation frequency are generated owing to two main sources of nonlinearity, namely material nonlinearity and CAN.

The material nonlinearity is caused by two strain components of the material: elastic and plastic [31]. The elastic component is caused by lattice anharmonicity while the plastic component is attributed to the local plasticity generated during cyclic loading. The relation between the stress perturbation and the elastic/plastic strain based on the nonlinear Hook's law can be written as [32]:

$$\text{Elastic: } \sigma = A_2^e \varepsilon_e + \frac{1}{2} A_3^e \varepsilon_e^2 + \dots, \quad (1)$$

$$\text{Plastic: } \sigma = A_2^{pl} \varepsilon_{pl} + \frac{1}{2} A_3^{pl} \varepsilon_{pl}^2 + \dots, \quad (2)$$

where  $A_2$  and  $A_3$  are Huang coefficients and  $\varepsilon$  is strain.

By considering the motion equation for one-dimensional wave in the Lagrangian coordinate system and equations (1) and (2), an acoustic nonlinearity parameter  $\beta$  is introduced to represent the material nonlinearity [32]:

$$\beta = \beta_e + \beta_{pl} = -\frac{A_3^e}{A_2^e} + \frac{16\pi^2 \Omega R^2 \Lambda h^3 (1-\nu)^2 (A_2^e)^2}{G^2 b}, \quad (3)$$

where  $\Omega$  and  $R$  denote two conversion factors from dislocation to longitudinal displacement and longitudinal to shear displacement in the slip plane, respectively,  $\Lambda$  is the dipole density,  $\nu$  is Poisson's ratio,  $G$  is the shear modulus and  $b$  is Burger's vector.

To experimentally measure material nonlinearity from inherent elasticity and local plasticity generated by fatigue damage, the equation of motion of a longitudinal wave in a solid medium is considered. By assuming that wave attenuation is negligible and taking the nonlinear relation between stress and total strain into account, the equation can be written as [33]:

$$\rho \frac{\partial^2 u}{\partial t^2} = E \frac{\partial^2 u}{\partial x^2} + E\beta \frac{\partial u}{\partial x} \frac{\partial^2 u}{\partial x^2}, \quad (4)$$

where  $\rho$  is the density of the medium,  $u$  is the displacement at time  $t$ ,  $x$  is the propagation distance,  $E$  is the elastic modulus of the material and  $\beta$  is the acoustic nonlinearity parameter.

Assuming a sinusoidal wave input with the angular frequency of  $\omega$  and wavenumber of  $k$ , a perturbation solution to equation (4) is:

$$u = A_1 \cos(kx - \omega t) + \frac{1}{8} \beta A_1^2 k^2 x \cos(2kx - 2\omega t) \\ = A_1 \cos(kx - \omega t) + A_2 \cos(2kx - 2\omega t). \quad (5)$$

Therefore, the measured acoustic nonlinearity parameter is defined as:

$$\beta = \frac{A_2}{A_1^2 k^2 x}, \quad (6)$$

where  $A_1$  and  $A_2$  are the magnitudes of the first order and second order harmonic waves respectively.

In general, a relative acoustic nonlinearity parameter  $\beta'$  is adopted [34–36] to monitor the variation of second harmonic due to the occurrence of fatigue crack:

$$\beta' = \frac{A_2}{A_1^2}. \quad (7)$$

On the other hand, the theory of CAN is based on the interaction between guided waves and the contact surfaces of a defect, e.g. a fatigue crack. In detail, the compressional part of the wave forces the crack surfaces to contact, allowing the wave to pass through, while the tensile part of the wave further opens the crack, blocking wave transmission and resulting in wave scattering [37]. This 'breathing' motion of the crack surfaces produces nonlinearity, e.g. higher harmonics, subharmonics, sidebands and frequency shift. The aforementioned interaction has been demonstrated

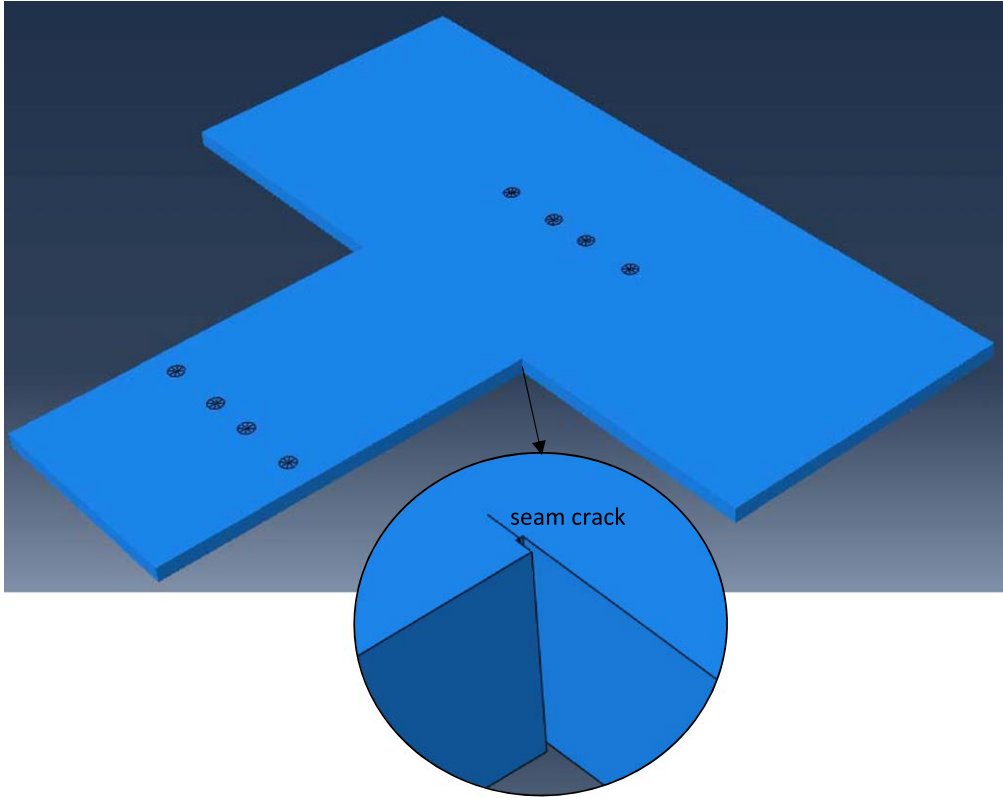


**Figure 3.** Simulation model of the steel joint.

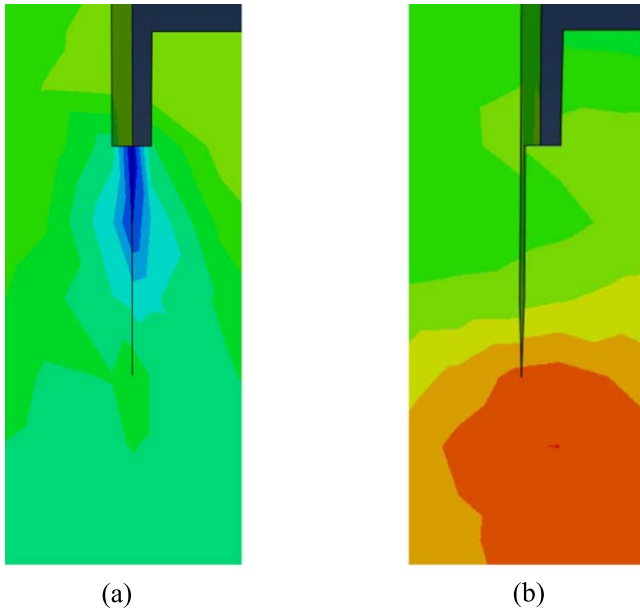


**Figure 4.** (a) Crack closed due to the compressive part of wave (b) crack opened due to the tensile part of wave.

analytically [38, 39] and numerically e.g. finite element method [34, 40] and local interaction simulation approach [41, 42]. Since equation (7) represents the material nonlinearity attributable to inherent elasticity and local plasticity generated by fatigue damage, a new relative acoustic

nonlinearity parameter  $\beta'_{CAN}$  was proposed recently for measuring CAN induced by micro-crack as:

$$\beta'_{CAN} = \frac{A_2}{A_1}. \quad (8)$$

Equation (8) can be derived on the basis of an enhanced bi-linear stiffness model by taking account of different effective moduli under tensile and compressive loadings [43] or an elastodynamic analysis by considering the displacement between the crack surfaces induced by the probing waves [39].

In view of the fact that the second harmonic measured in experiments is comprised of both material nonlinearity and CAN, the classical acoustic nonlinearity parameter  $\beta'$  in equation (7) is still widely adopted by many researchers [34–36, 44–47] to investigate fatigue crack. In this study,  $\beta'$  will be exploited to quantify the variation of total nonlinearity owing to the presence of fatigue crack. The difference between  $\beta'$  and  $\beta'_{CAN}$  will be discussed in section 4.

### 3. Numerical studies

#### 3.1. Modelling

The geometry of a steel joint 10 mm in thickness with two through-thickness notches each 1 mm in length at both corners from which the crack would initiate and propagate is illustrated in figure 1. Piezoelectric actuators ( $A_1$ – $A_4$ ) and receivers ( $R_1$ – $R_4$ ) were located on the flange and web of the



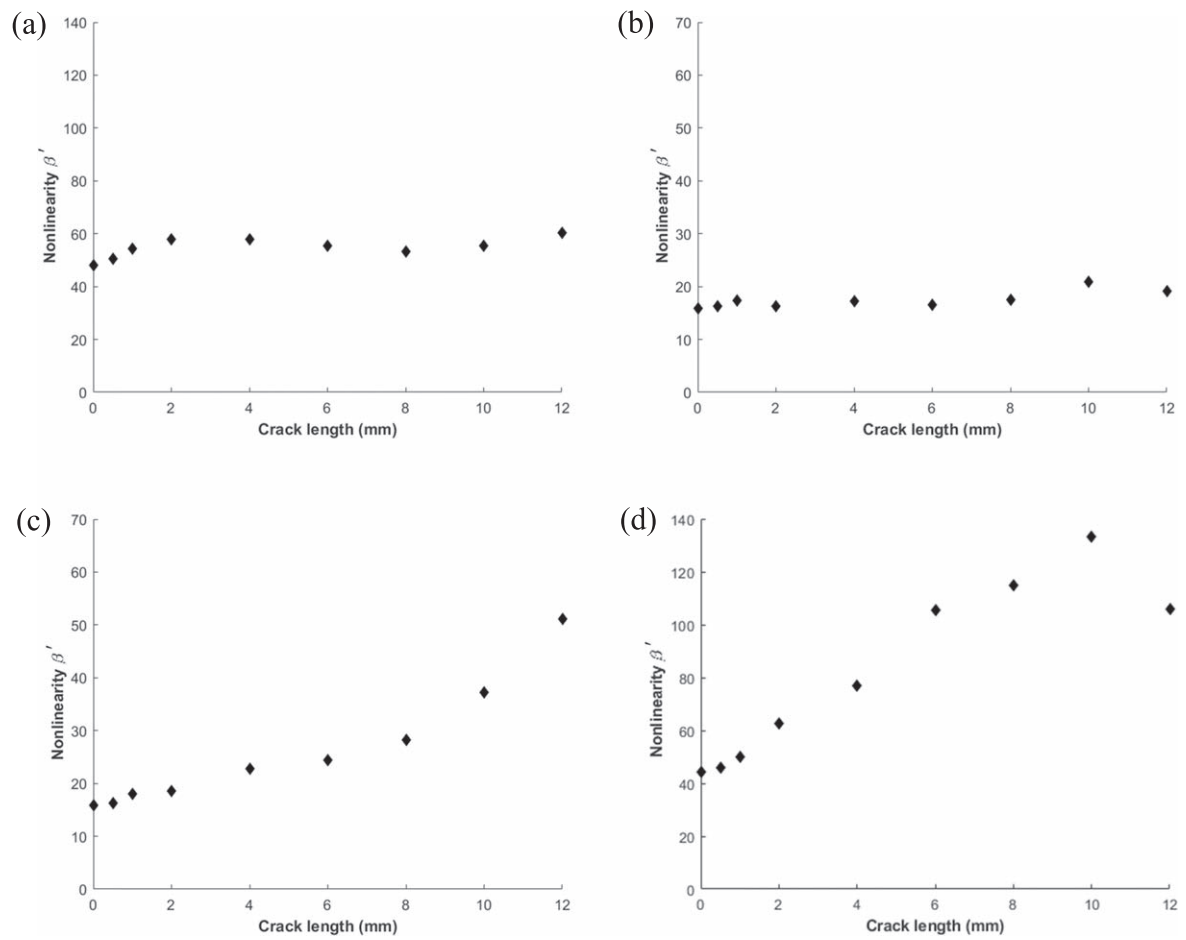


**Figure 5.** Nonlinearity parameter against crack length in simulation (a) sensing path 1, (b) sensing path 2, (c) sensing path 3 and (d) sensing path 4.

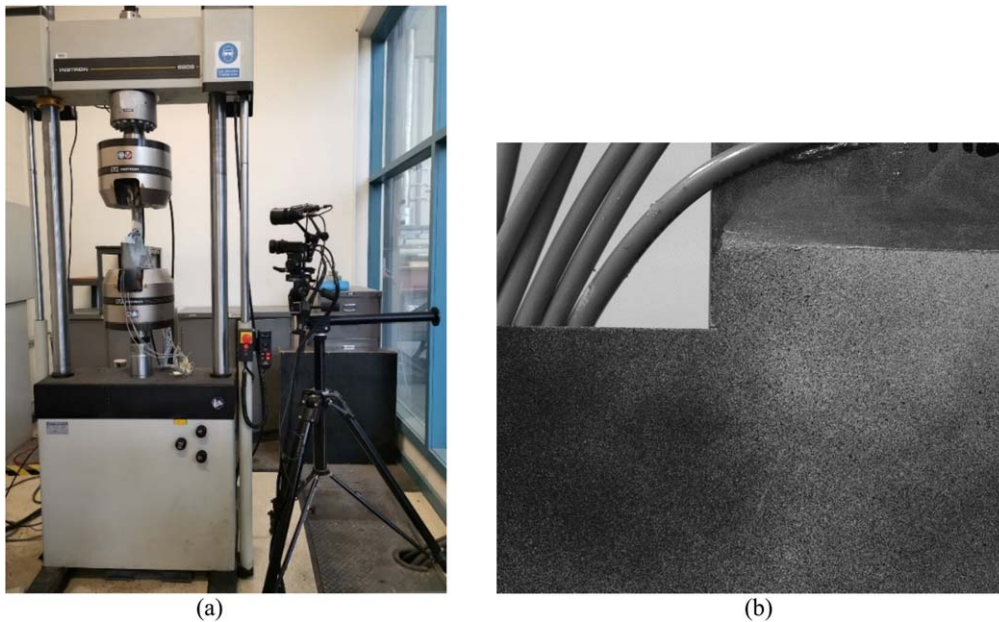


**Figure 6.** Experimental setup (a) fatigue machine and DIC system (b) speckle pattern.

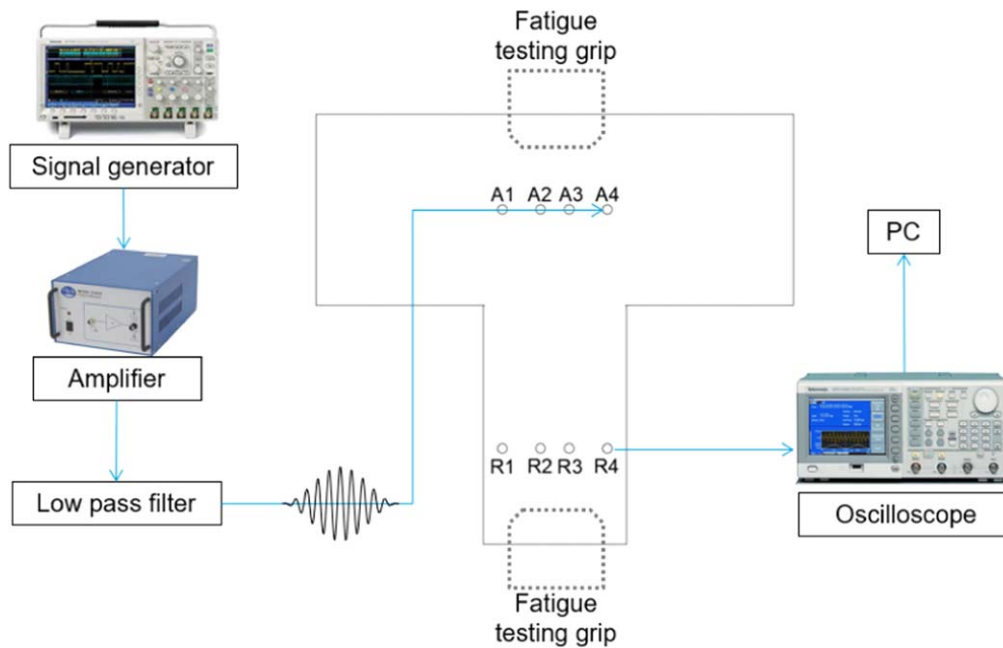


Figure 7. Signal acquisition system.

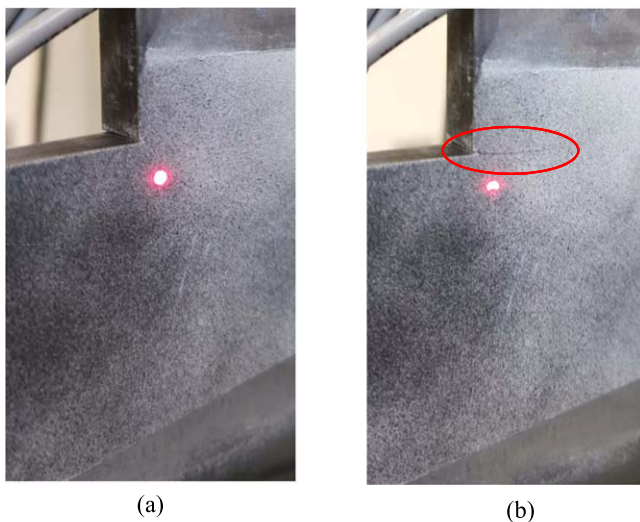


Figure 8. Fatigue crack after 340 000 loading cycles (a) unloaded (b) loaded.

specimen respectively. The material properties of the specimen are given in table 1.

To generate a cumulative second harmonic, the fundamental and double frequencies of the guided wave mode should have comparable group and phase velocities which satisfy two conditions, namely synchronism and non-zero flux [48]. Even though they are generally for the accumulation of material nonlinearity, these conditions have been widely utilised to investigate total nonlinearity induced by fatigue damage studies [35, 44, 49, 50] where CAN dominates the variation of total nonlinearity. In this study, a Hanning windowed 10-cycle sine wave burst at 377 kHz was chosen as the excitation signal to generate S1 mode based on the dispersion curves, calculated for a 10 mm thick steel plate (figure 2), while S2 mode at 754 kHz is generated after S1

interacts with the crack. At the selected frequencies, S1 and S2 modes have the fastest velocities among all modes, separating them clearly from other modes (S0, A0, A1 and A2).

Simulation of the steel joint was performed using the commercial FE package ABAQUS<sup>®</sup> Dynamic/Explicit. The specimen was meshed using eight-node brick elements (C3D8R). The actuators and sensors were modelled as circular planes partitioned from the surface of the plate as shown in figure 3. The element size was set at 0.6 mm and the time increment was specified as 1.2e-8 s. The built-in function 'seam' in ABAQUS was assigned to each surface of the crack to mimic a fatigue crack. In addition, 'hard' contact and small relative sliding were allocated as the interactions between the two crack surfaces to minimise penetration of the surfaces. Since it had been noticed that the variation of total nonlinearity is dominated by CAN for the scenario of fatigue crack whereas the contribution due to material nonlinearity is minimal [11, 47], material nonlinearity was not considered in the simulation in this study for simplicity while the total nonlinearity including CAN and material nonlinearity is still measured in experiments.

### 3.2. Simulation results

Based on the experimental results to be detailed in the following section, a fatigue crack of various lengths ranging from 0 to 12 mm with the maximum increment of 2 mm was simulated on the notch near sensing path 4. The simulated CAN mechanism for a typical crack is demonstrated in figure 4, where the crack is closed by the compressive part of the wave (figure 4(a)) and opened by the tensile part of the wave (figure 4(b)). Consequently, the combined 'open and closed' motion of the crack generates higher harmonics.

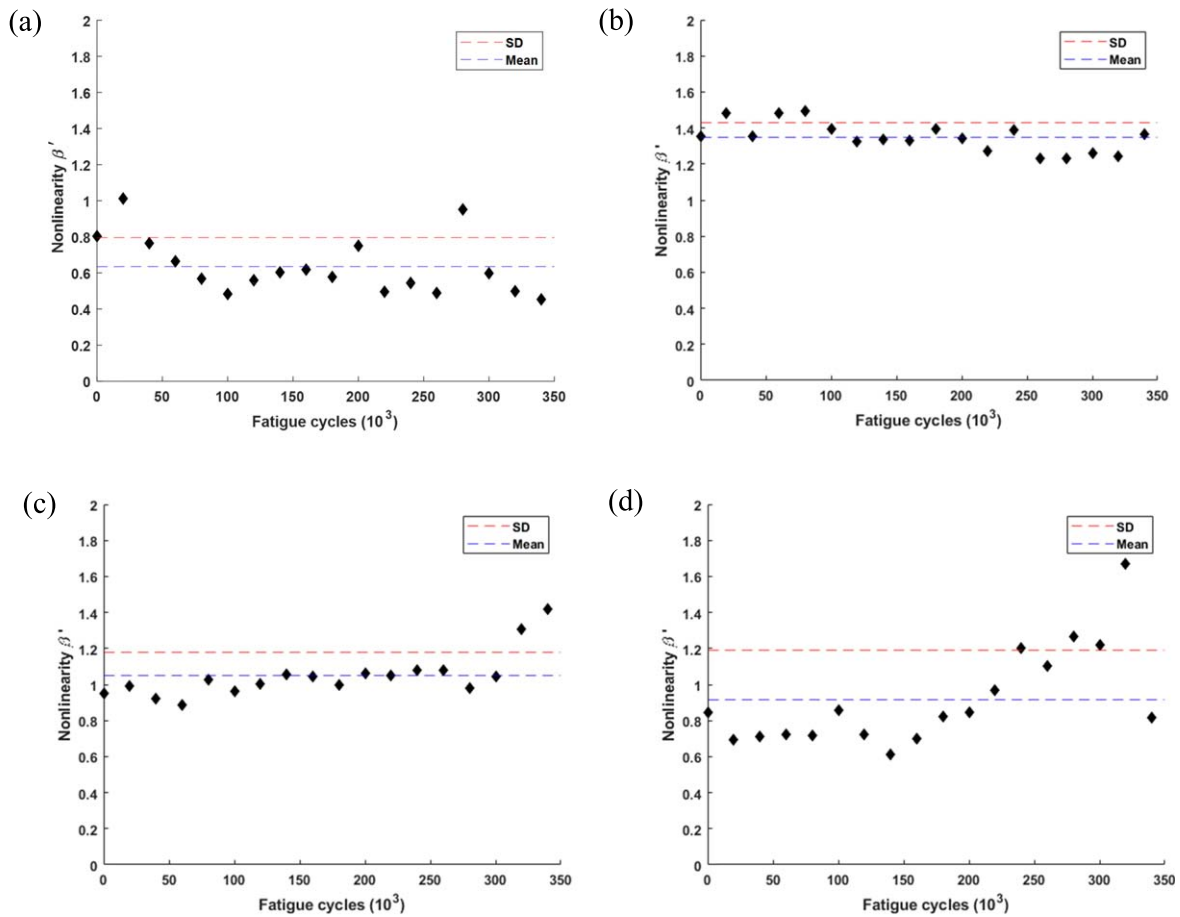


**Figure 9.** Variations of nonlinearity with respect to the number of fatigue loading cycles (a) sensing path 1, (b) sensing path 2, (c) sensing path 3 and (d) sensing path 4.

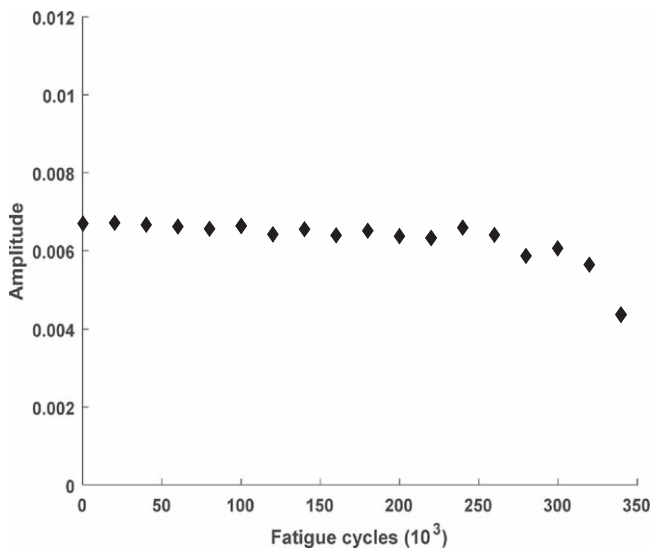


**Figure 10.** Variations of amplitude of fundamental frequency with respect to the number of fatigue loading cycles of sensing path 4.

To calculate the nonlinearity, the received signals were processed by a fast Fourier transform (FFT) algorithm to extract the wave amplitudes at the fundamental frequency and second harmonic. The results of sensing path 4 (figure 1) present an obvious increase in nonlinearity up to the crack

length of 10 mm as shown in figure 5(d). The surge in nonlinearity proves the sensitivity of nonlinear guided waves for recognising the variation in crack length. Once the crack grows relatively large, it is difficult to close the two crack surfaces, so the contact area is lessened [20]. Consequently, the guided waves are less likely to propagate through the crack, which causes a decline in nonlinearity as shown in figure 5(d) for the crack length of 12 mm. Furthermore, it is observed that sensing path 3 is also affected by the growth of the fatigue crack, as depicted in figure 5(c), where a gradual rise in nonlinearity and a significant growth occur at the crack length of 10 mm. In contrast, the variation in nonlinearity detected by sensing paths 1 and 2, as shown in figures 5(a), (b), are substantially lower and remain relatively constant compared to sensing paths 3 and 4, due to the greater distance from the crack location.

## 4. Experimental study

### 4.1. Setup

Experiments were conducted to monitor crack initiation and growth on a steel joint subjected to tensile cyclic loading. The steel joint was Grade 350 which had yield strength and tensile strength similar to those of the steel [51] used in bogie frames.



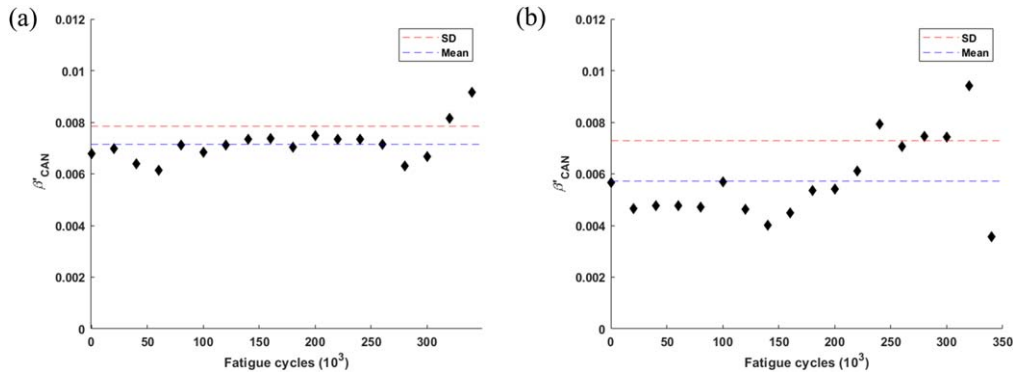


**Figure 11.** Variations of  $\beta'_{CAN}$  with respect to the number of fatigue loading cycles (a) sensing path 3 and (b) sensing path 4.

The specimen was 10 mm thick. Two 1 mm through-thickness notches were machined at both corners in order to produce a local stress concentration and facilitate the development of a micro-crack. The specimen was gripped in the jaws of an Instron 8802 fatigue machine (figure 6(a)). The maximum stress applied was 150 MPa, which was approximately 33% of the ultimate tensile strength and 43% of the yield strength of the notched specimen. In order to apply tensile cyclic loading, the stress ratio was set at 0.1, i.e. the stress ranged from 150 to 15 MPa, and the testing frequency was 10 Hz.

Figure 7 represents the data acquisition system comprised of 10 mm circular piezoelectric transducers (PZTs) functioning as both actuators and receivers bonded on the upper surface, a Tektronix AFG 3102 function generator, a Trek 2100HF amplifier, a low pass filter to minimise noise induced by instruments and a Tektronix DPO 4034B oscilloscope connected to the receivers to collect signals. Nonlinear ultrasonic measurement was performed every 20 000 cycles. The excitation signal was the same as that used in simulation. The responses were acquired at a sampling frequency of 500 MHz after averaging 512 samples.

In order to validate the results based on the second harmonic approach, DIC was implemented by utilising the ARAMIS non-contact optical deformation measuring system (figure 6). To implement DIC, the object surface requires speckle patterns, either natural or artificial, to be able to perform correlation computations. To this end, a speckle pattern was applied on the top surface around the notch areas by spraying white and black paint (figure 6(b)), which allowed the system to measure the surface displacement. The digital images recorded before and after deformation were partitioned into virtual subsets. A deformed position of one subset was determined by correlating an undeformed subset with deformed subsets and selecting the one that yielded the peak correlation coefficient. Consequently, variation in the positions of the subsets was exploited to calculate the in-plane displacement. Since fatigue crack initiation and growth result in surface displacement, DIC could precisely diagnose the crack initiation and trajectory.

#### 4.2. Experimental results

The specimen was subjected to the fatigue load of 340 000 cycles in total and a hairline fatigue crack as highlighted in figures 8(a), (b) was generated at the notch near sensing path 4 only instead of occurring at both corners, which was acceptable for experimental testing. The signals acquired by nonlinear ultrasonic measurement were converted to the frequency domain by an FFT to obtain the amplitudes at fundamental and second harmonic frequencies. The nonlinearity was then calculated using equation (7). The results of nonlinearity at various loading cycles and the mean and standard deviation (SD) values of the nonlinearities of each path are depicted in figures 9(a)–(d). It is evident that the nonlinearity of sensing path 4 begins to increase at around 220 000 cycles, whereas the other sensing paths remain steady at this number of cycles, which signifies the initiation of a fatigue crack near sensing path 4. Meanwhile, the change in amplitude at fundamental frequency is minimal, as shown in figure 10. After that, an upward trend can be clearly observed for sensing path 4 up to 320 000 cycles where the nonlinearities exceed the SD, implying further growth of the fatigue crack. The significant decrease in nonlinearity at 340 000 cycles in figure 9(d) indicates that the crack has grown to such an extent that the waves cannot penetrate and less CAN effect is induced. In fact, it is noticed that the signal received at the fundamental frequency begins to show a substantial change at this number of cycle, exemplified by the signal amplitude on sensing path 4 (figure 10). It can be inferred that the sensitivity of the linear guided wave is limited to macro-damage whereas the nonlinear guided wave is capable of characterising crack at the incipient stage.

It is also notable in figure 9(c) that the nonlinearity of sensing path 3 increases above its SD value at 320 000 cycles and continues to increase until 340 000 cycles. That feature reveals that the crack has extended to the region of sensing path 3 and nonlinearity due to the CAN effect generated at the crack tip begins to affect the signal. For sensing path 2, as shown in figure 9(b), the nonlinearity remains steady over the entire period with a few points slightly above SD at the very beginning of the fatigue cycles, indicating a negligible effect of the fatigue crack. It is noteworthy that the nonlinearity of sensing path 1 also remains relatively constant except at

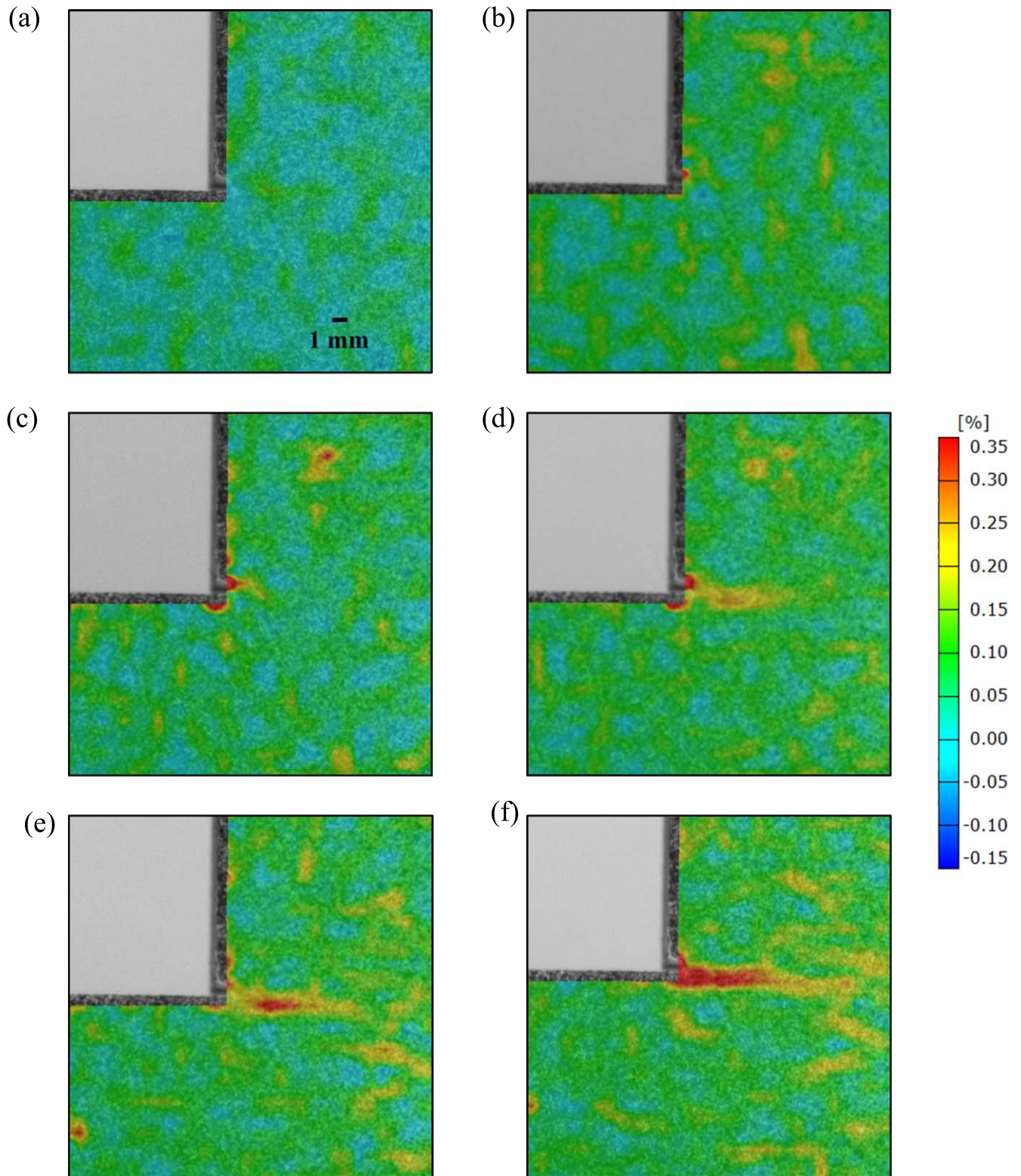


**Figure 12.** Strain field measured by DIC after different fatigue loading cycles (a) benchmark, (b) 200 000 cycles (c) 220 000 cycles, (d) 300 000 cycles, (e) 320 000 cycles and (f) 340 000 cycles.

20 000 and 280 000 cycles as shown in figure 9(a). These outliers may have several causes, e.g. measurement error or background noise. As well, the fluctuation in nonlinearity may be attributed to the plastic zone of the notch generated near sensing path 1, which however does not fully evolve into

the formation and propagation of fatigue crack as the test progresses. As a result, the nonlinearity shows irregularity, unlike the monotonic behaviour of its counterpart near sensing path 4 where the fatigue crack develops.

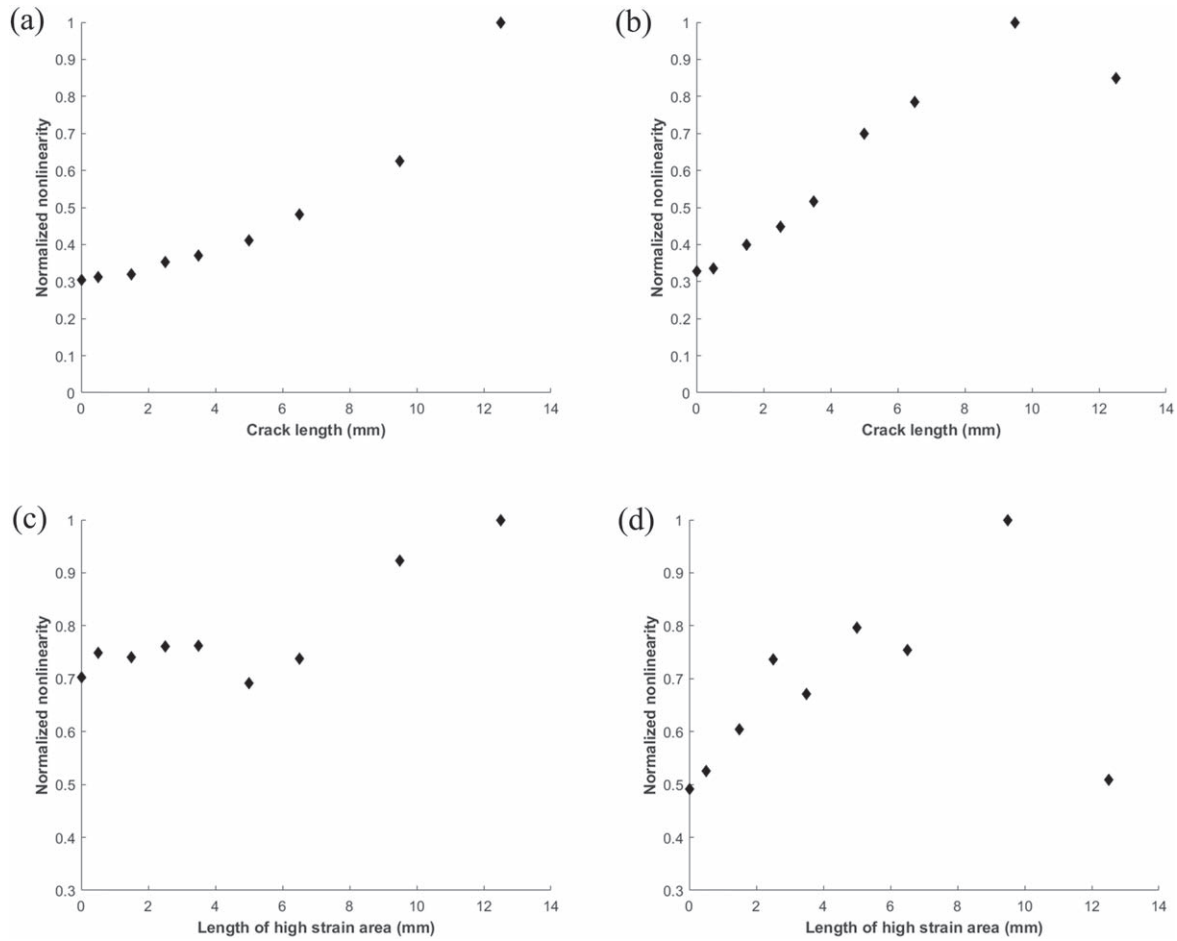


**Figure 13.** Normalised nonlinearity (numerical) versus crack length for (a) sensing path 3 (b) sensing path 4 and normalised nonlinearity (experimental) versus length of high-strain area for (c) sensing path 3 (d) sensing path 4.

As a comparison, the results represented by  $\beta'_{CAN}$  for sensing paths 3 and 4 are depicted in figure 11 because these two paths are significantly affected by fatigue crack. It is observed that the trend of  $\beta'_{CAN}$  is quite similar to that of  $\beta'$ , where both indicate a rise of nonlinearity at 220 000 cycles and a significant decrease at 340 000 cycles due to the considerable crack growth. Since the signal magnitude at the fundamental frequency ( $A_1$ ) starts to decrease as shown in figure 10, the drop of both  $\beta'$  and  $\beta'_{CAN}$  at 340 000 cycles implies more significant magnitude decrease in the second order harmonic ( $A_2$ ) according to their respective definitions in equations (7) and (8). In the consideration of the fact that the second harmonic nonlinearity measured in experiments consists of both material nonlinearity and CAN, the decrease in  $A_2$  is mainly attributable to the substantial disappearance of CAN as material nonlinearity including inherent elasticity and local plasticity generated by fatigue damage is not expected to decrease with increase of crack size. Such an observation further proved that CAN dominates the total nonlinearity for the scenario of fatigue crack whereas the contribution from material nonlinearity is minimal. Therefore,  $\beta'$  can still be used as an indicator to represent the initiation and growth of fatigue crack. It is also interesting to notice that  $\beta'_{CAN}$  appears

more sensitive than  $\beta'$  to represent CAN as the change in  $\beta'_{CAN}$  at 340 000 cycles is greater than that in  $\beta'$  in terms of their respective mean values.

In parallel, images from the DIC system were recorded during the unloaded stage at the same interval of ultrasonic measurements. The strain shown in figure 12 is the major strain based on a combination of all in-plane strains, i.e. normal and shear strains. As shown in figures 12(a)–(f), it is evident that the images showing strain field are in good agreement with the ultrasonic measurements of sensing path 4. At 200 000 cycles, the high-strain area is concentrated at the notch tip, as indicated in red in figure 12(b) compared to its vicinity and figure 12(a) representing the status before the test as benchmark. The high-strain area then expands further to the right at 220 000 cycles (see figure 12(c)). The fatigue crack propagation can subsequently be observed in figures 12(d)–(f) based on the change in local strains around the notch. It is evident in figure 12(f) that the surface displacement has become sufficient large, which correlates well with the significant drop in nonlinearity at 340 000 cycles where the waves could not transmit through the crack because of the large displacement.



## 5. Discussion

As the images from DIC correlated well with the ultrasonic measurements, the normalised nonlinearities of sensing paths 3 and 4 were plotted against the length of the high-strain area based on DIC images which were measured with the threshold of 0.195% at different fatigue cycles. The results were then compared with the numerical results, as shown in figures 13(a)–(d), where a similar trend of nonlinearity change in terms of crack length can be observed. In detail, for sensing path 4, an overall ascending trend of nonlinearity is evident up to the crack length of 9.5 mm, with a subsequent rapid descent, whereas for sensing path 3, a substantial increase in nonlinearity begins at the crack length of 9.5 mm. Besides, the substantial drop in amplitude of fundamental frequency at 340 000 cycles shown in figure 10 can be explained by the fact that the crack length according to DIC measurement is 12.5 mm, which can be considered as a macro damage in comparison with the wavelength (12.2 mm) of the excited wave mode. It is therefore concluded that the fatigue crack can be approximately quantified using the nonlinear ultrasonic method with the assistance of the DIC technique.

On the other hand, it should be understood that DIC is expensive and complex to implement for practical engineering applications. First, an additional layer of speckle pattern deposited on the steel surface is necessary in order to obtain the surface deformation. However, surface degradation due to weathering and oxidation is likely to occur, which can result in a false alarm or error in computation. Second, the inaccessibility of certain regions of engineering structures such as the bogie frame also prevents cost-effective application of DIC. In contrast, real-time identification and quantification of fatigue crack initiation and propagation can be achieved by installing affordable PZT sensors on these difficult-to-access and difficult-to-inspect regions during service of the structure.

## 6. Conclusion

Nonlinear Lamb waves were numerically and experimentally studied for fatigue crack evaluation in a steel joint by means of the second harmonic method, where a DIC system was implemented to support observations from the guided-waves-based method. The effect of fatigue crack growth on nonlinearity was simulated by increasing the length of a seam crack in the numerical study. PZTs were surface-bonded on the steel joint in the experimental study to generate and receive wave signals and four sensing paths were arranged to observe the development of fatigue crack. During fatigue testing, the surface deformation was captured by a DIC system to monitor the growth of the fatigue crack.

Both numerical simulation and experimental testing successfully captured the CAN caused by fatigue crack initiation and growth. In particular, the experimental results showed good consistency with the DIC images. The length of the high-strain area indicating the extent of the crack was further extracted from the DIC images at different fatigue cycles to correlate the numerical and experimental results,

revealing good agreement in terms of crack development. It was therefore concluded that nonlinear guided waves could identify fatigue crack initiation and quantify its growth at micro-damage level until it developed into macro-damage. Further study will investigate the influence of various operating conditions of bogie frames such as vibration, temperature variation, and the effect of co-existence of corrosion on nonlinear guided waves.

## Acknowledgments

The authors greatly appreciate the financial support from the Rail Manufacturing Cooperative Research Centre (funded jointly by participating rail organisations and the Australian Federal Government's Business Cooperative Research Centres Program) through Project R3.7.5-Nonlinear vibro-acousto-ultrasonic waves for fatigue cracking detection in key rail components.

## ORCID iDs

Ye Lu  <https://orcid.org/0000-0002-2319-7681>

## References

- [1] Avery R, Mcauley J and 2018 Trainline 6 *Statistical Report* Bureau of Infrastructure, Transport and Regional Economics (BITRE), Canberra ACT [https://www.bitre.gov.au/sites/default/files/train\\_006.pdf](https://www.bitre.gov.au/sites/default/files/train_006.pdf)
- [2] RailCorp 2010 RailCorp Engineering Standard — Rolling Stock, ESR 0540 : OVERHAUL OF 48 CLASS LOCOMOTIVE BOGIES. Australia. [https://www.transport.nsw.gov.au/system/files/media/asa\\_standards/2017/esr-0540.pdf](https://www.transport.nsw.gov.au/system/files/media/asa_standards/2017/esr-0540.pdf)
- [3] Barke D and Chiu W 2005 Structural health monitoring in the railway industry: a review *Struct. Health Monit.* **4** 81–93
- [4] Wang D *et al* 2012 Monitoring of delamination onset and growth during mode I and mode II interlaminar fracture tests using guided waves *Compos. Sci. Technol.* **72** 145–51
- [5] Lu Y, Ye L and Su Z 2006 Crack identification in aluminium plates using Lamb wave signals of a PZT sensor network *Smart Mater. Struct.* **15** 839
- [6] Li J *et al* 2017 Guided waves for debonding identification in CFRP-reinforced concrete beams *Constr. Build. Mater.* **131** 388–99
- [7] Hayashi T and Murase M 2005 Defect imaging with guided waves in a pipe *J. Acoust. Soc. Am.* **117** 2134–40
- [8] Wilcox P *et al* 2003 Long range inspection of rail using guided waves *AIP Conf. Proc.* **657** 236–43
- [9] Zhao X *et al* 2007 Active health monitoring of an aircraft wing with embedded piezoelectric sensor/actuator network: I. Defect detection, localization and growth monitoring *Smart Mater. Struct.* **16** 1208
- [10] Shen Y, Wang J and Xu W 2018 Nonlinear features of guided wave scattering from rivet hole nucleated fatigue cracks considering the rough contact surface condition *Smart Mater. Struct.* **27** 105044
- [11] Guan R *et al* 2019 Fatigue crack detection in pipes with multiple mode nonlinear guided waves *Struct. Health Monit.* **18** 180–92

- [12] Zhang J and Xuan F-Z 2014 Fatigue damage evaluation of austenitic stainless steel using nonlinear ultrasonic waves in low cycle regime *J. Appl. Phys.* **115** 204906
- [13] Jeon I *et al* 2019 Fatigue crack detection in rotating steel shafts using noncontact ultrasonic modulation measurements *Eng. Struct.* **196** 109293
- [14] Yelve N P, Mitra M and Mujumdar P 2017 Detection of delamination in composite laminates using Lamb wave based nonlinear method *Compos. Struct.* **159** 257–66
- [15] Tian Y *et al* 2019 Metamaterial improved nonlinear ultrasonics for fatigue damage detection *Smart Mater. Struct.* **28** 075038
- [16] Wang Y, Guan R and Lu Y 2017 Nonlinear Lamb waves for fatigue damage identification in FRP-reinforced steel plates *Ultrasonics* **80** 87–95
- [17] Yang Y, Ng C-T and Kotousov A 2019 Bolted joint integrity monitoring with second harmonic generated by guided waves *Struct. Health Monit.* **18** 193–204
- [18] Lim H J and Sohn H 2019 Online fatigue crack prognosis using nonlinear ultrasonic modulation *Struct. Health Monit.* **18** 1889–1902
- [19] Li N *et al* 2016 Quantitative evaluation of micro-cracks using nonlinear ultrasonic modulation method *NDT E Int.* **79** 63–72
- [20] Guan R *et al* 2018 Quantitative fatigue crack evaluation in pipeline structures using nonlinear cylindrical waves *Smart Mater. Struct.* **28** 025015
- [21] Pan B *et al* 2009 Two-dimensional digital image correlation for in-plane displacement and strain measurement: a review *Meas. Sci. Technol.* **20** 062001
- [22] Carroll J D *et al* 2013 High resolution digital image correlation measurements of strain accumulation in fatigue crack growth *Int. J. Fatigue* **57** 140–50
- [23] Giancane S *et al* 2010 Fatigue damage evolution of fiber reinforced composites with digital image correlation analysis *Procedia Eng.* **2** 1307–15
- [24] Ghorbani R, Matta F and Sutton M A 2015 Full-field deformation measurement and crack mapping on confined masonry walls using digital image correlation *Exp. Mech.* **55** 227–43
- [25] Pan B *et al* 2010 High-temperature digital image correlation method for full-field deformation measurement at 1200 C *Meas. Sci. Technol.* **22** 015701
- [26] Zhang R and He L 2012 Measurement of mixed-mode stress intensity factors using digital image correlation method *Opt. Lasers Eng.* **50** 1001–7
- [27] Moreira D *et al* 2012 Determination of Young's modulus in polyester-Al<sub>2</sub>O<sub>3</sub> and epoxy-Al<sub>2</sub>O<sub>3</sub> nanocomposites using the digital image correlation method *Composites A* **43** 304–9
- [28] Kumar R V, Bhat M and Murthy C 2013 Evaluation of kissing bond in composite adhesive lap joints using digital image correlation: preliminary studies *Int. J. Adhes. Adhes.* **42** 60–8
- [29] Shirole D, Hedayat A and Walton G 2019 Experimental relationship between compressional wave attenuation and surface strains in brittle rock *J. Geophys. Res.: Solid Earth* **124** 5770–93
- [30] Omondi B *et al* 2016 Improved crack monitoring in structural concrete by combined acoustic emission and digital image correlation techniques *Struct. Health Monit.* **15** 359–78
- [31] Masurkar F, Peter W T and Yelve N 2018 Investigating the critical aspects of evaluating the material nonlinearity in metal plates using Lamb waves: theoretical and numerical approach *Appl. Acoust.* **140** 301–14
- [32] Cantrell J H and Yost W T 2001 Nonlinear ultrasonic characterization of fatigue microstructures *Int. J. Fatigue* **23** 487–90
- [33] Kim J-Y *et al* 2006 Experimental characterization of fatigue damage in a nickel-base superalloy using nonlinear ultrasonic waves *J. Acoust. Soc. Am.* **120** 1266–73
- [34] Hong M *et al* 2014 Modeling nonlinearities of ultrasonic waves for fatigue damage characterization: theory, simulation, and experimental validation *Ultrasonics* **54** 770–8
- [35] Zhou C *et al* 2012 Evaluation of fatigue cracks using nonlinearities of acousto-ultrasonic waves acquired by an active sensor network *Smart Mater. Struct.* **22** 015018
- [36] Yang Y *et al* 2018 Second harmonic generation at fatigue cracks by low-frequency Lamb waves: experimental and numerical studies *Mech. Syst. Sig. Process.* **99** 760–73
- [37] Jhang K-Y 2009 Nonlinear ultrasonic techniques for nondestructive assessment of micro damage in material: a review *Int. J. Precis. Eng. Manuf.* **10** 123–35
- [38] Solodov I Y, Krohn N and Busse G 2002 CAN: an example of nonclassical acoustic nonlinearity in solids *Ultrasonics* **40** 621–5
- [39] Wang K *et al* 2019 Nonlinear aspects of 'breathing' crack-disturbed plate waves: 3D analytical modeling with experimental validation *Int. J. Mech. Sci.* **159** 140–50
- [40] Kawashima K *et al* 2002 Nonlinear acoustic response through minute surface cracks: FEM simulation and experimentation *Ultrasonics* **40** 611–5
- [41] Shen Y and Cesnik C E 2017 Modeling of nonlinear interactions between guided waves and fatigue cracks using local interaction simulation approach *Ultrasonics* **74** 106–23
- [42] Shen Y and Cesnik C E 2018 Local interaction simulation approach for efficient modeling of linear and nonlinear ultrasonic guided wave active sensing of complex structures *J. Nondestruct. Eval., Diagn. Prognostics Eng. Syst.* **1** 011008
- [43] Zhao Y *et al* 2016 A micromechanics model for the acoustic nonlinearity parameter in solids with distributed microcracks *AIP Conf. Proc.* **1706** 060001
- [44] Pruell C *et al* 2009 Evaluation of fatigue damage using nonlinear guided waves *Smart Mater. Struct.* **18** 035003
- [45] Yang Y, Ng C-T and Kotousov A 2018 Influence of crack opening and incident wave angle on second harmonic generation of Lamb waves *Smart Mater. Struct.* **27** 055013
- [46] Lee T H and Jhang K Y 2009 Experimental investigation of nonlinear acoustic effect at crack *NDT E Int.* **42** 757–64
- [47] Wang R *et al* 2019 Nonlinear ultrasonic detection for evaluating fatigue crack in metal plate *Struct. Health Monit.* **18** 869–81
- [48] Deng M 2003 Analysis of second-harmonic generation of Lamb modes using a modal analysis approach *J. Appl. Phys.* **94** 4152–9
- [49] Su Z *et al* 2014 Acousto-ultrasonics-based fatigue damage characterization: linear versus nonlinear signal features *Mech. Syst. Sig. Process.* **45** 225–39
- [50] Hong M *et al* 2015 Locating fatigue damage using temporal signal features of nonlinear Lamb waves *Mech. Syst. Sig. Process.* **60** 182–97
- [51] Yoon S C *et al* 2013 A study on the characteristics of Bogie frame materials *Appl. Mech. Mater.* **420** 144–8